Journal of Materials Chemistry A

Accepted Manuscript

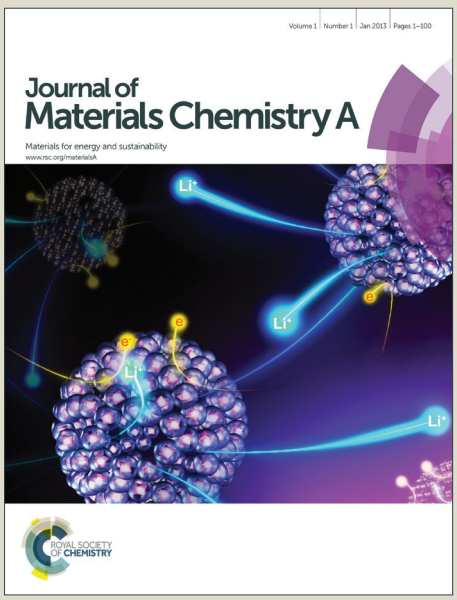

ROYAL SOCIETY OF CHEMISTRY

www.rsc.org/materialsA

Sorption Interactions of Plutonium and Europium with Ordered Mesoporous Carbon

Tashi Parsons-Moss[1,2], Jinxiu Wang[3], Stephen Jones[1,2], Erin May[1,2] , Daniel Olive[1,2], Zurong Dai[4], Mavrik Zavarin[4], Annie B. Kersting[4] , Dongyuan Zhao[3], and Heino Nitsche[1,2]

[1]Department of Chemistry, University of California, Berkeley, Berkeley, CA 94720, USA

[2]Nuclear Science Division, Lawrence Berkeley National Laboratory, Berkeley, CA 94720, USA

[3]Department of Chemistry and Laboratory of Advanced Materials, Fudan University, Shanghai 200433 (P.R. China)

[4]Lawrence Livermore National Laboratory, Glenn T Seaborg Institute, Livermore, CA 94550 USA

Abstract: Both 3d-cubic FDU-16-type and 2d-hexagonal C-CS-type ordered mesoporous carbons (OMCs) were synthesized to test their application as radionuclide sorbent materials. A portion of each OMC was oxidized with acidic ammonium persulfate (APS), and the physicochemical properties of all four OMCs were characterized with several techniques. Based on plutonium (Pu) sorption and desorption tests with FDU-16, oxidized FDU-16-COOH, C-CS, and oxidized C-CS-COOH, the C-CS-COOH was the most effective OMC for sorption of Pu over a wide pH range. Batch sorption interactions of C-CS and C-CS-COOH were further explored with Pu(VI) and Eu(III) to determine the uptake capacities, sorption kinetics, and effects of ionic strength. The nature of the Pu sorption reaction was also probed via X-ray absorption spectroscopy (XAS) and transmission electron microscopy (TEM). The highly oxidized surface, large pores, and high surface area of C-CS-COOH make it a very effective general scavenger for actinide and lanthanide cations. Pu and Eu uptake by C-CS-COOH appears to be dictated by chemisorption, and the Langmuir Eu capacity (138 mg/g from pH 4 solution) is higher than those previously reported for many other adsorbents. Pristine C-CS has a low affinity for Eu(III), but is an excellent sorbent of PuO_2 nanocrystals (~ 3 nm diameter), which are formed because the carbon reduces Pu(VI) and Pu(V) to Pu(IV). Plutonium is also reduced by C-CS-COOH, but PuO_2 colloid formation in pH 4 solution is prevented by carboxyl complexation of Pu(IV) at the C-CS-COOH surface.

1. Introduction

The current stockpile of Pu in the biosphere coupled with its radiotoxicity and long half-life (^{239}Pu $t_{1/2}$ = 24,100 years) makes this actinide a great environmental concern. Plutonium is a component of spent nuclear fuel, and thus a potential

contaminant in the event of a spill or leak from a storage tank or nuclear reactor accident. Significant amounts of ^{239}Pu have been released into the environment via nuclear weapons production and testing, nuclear reactor accidents, and incidents during the transport of nuclear weapons.[1-3] The chemistry of Pu is very complex, with four stable oxidation states available under various environmental conditions.[4, 5] The higher oxidation states (Pu(V) and Pu(VI)) exist in solution as PuO_2^+ and PuO_2^{2+} and are generally much more soluble than the lower oxidation states (Pu(IV) and Pu(III)). This makes them more mobile in oxic environments. Tetravalent Pu is readily hydrolyzed in environments with a pH greater than one and forms intrinsic Pu oxide colloids, which enhance its mobility through the environment.[6] Therefore, the investigation of high-capacity adsorbent materials for sequestration of oxidized and colloidal forms of Pu is important for stewardship surrounding the use of nuclear power. The sorption of europium (Eu) is also of concern, as this toxic metal has been released into the environment via fallout from nuclear explosions and accidents[7], nuclear waste discharge[7], petroleum-producing industries[8], and improper disposal of household appliances[8]. Europium, like the other lanthanides, is stable as a trivalent cation over a wide range of aqueous conditions, and is often used as a representative analog for trivalent actinides.[9] Both lanthanides and actinides generally behave as hard acids, although the actinides can show slightly more co-valency in their interaction with ligands and surfaces.

In recent years, carbonaceous materials have attracted attention for applications involving actinide and lanthanide sorption, as these materials are generally inexpensive and chemically stable under a wide range of conditions. Several variations of activated carbon have been employed for the sequestration of uranium (U(VI))[10-18] and Eu(III)[7, 8, 19]. Most of those studies found moderate to low sorption capacities. Although activated carbons have large pore volumes and surface areas, they tend to be disordered, with variable pore sizes. Carbon nanotubes are more uniform and have been explored for actinide and lanthanide extraction [20-27], but their uptake capacities may be limited by relatively low specific surface areas. Most recently graphene oxide has been studied for sorption of Eu(III)[28, 29] and other radionuclides[29], showing improved uptake kinetics and sorption capacities compared to nanotubes and activated carbons. Ordered mesoporous carbons (OMCs) are another class of carbonaceous materials that are attractive as sorbents because of their extremely high surface areas, large pore volumes, open frameworks, and highly ordered, tunable structures. Only recently have OMCs gained attention as possible sorbents for actinides and lanthanides. In the last three years several publications have appeared concerning functionalized OMCs for adsorption of U(VI) from seawater[30-33] and other aqueous solutions.[34-41] Much higher U(VI) sorption capacities have been achieved with functionalized[30, 34, 35, 41], oxidized[39], and untreated[40] OMCs, than with activated carbons[10, 18] or carbon nanotubes[26, 27].

We recently reported the first study of an OMC material for sorption of a transuranic element, in which Pu uptake by CMK-type mesoporous carbon, both untreated and oxidized by nitric acid treatment, was compared to that by a commercial activated carbon powder.[42] Both untreated and oxidized CMK materials greatly outperformed activated carbon in terms of Pu sorption kinetics and uptake capacity, and showed much greater sorption capacity than the carbon nanotube material that was

examined for Pu sorption previously.[22] In samples with high Pu concentration (250 μM Pu(VI/V) in pH 4 solution) the Pu uptake kinetics and apparent capacities for Pu sorption were the same for the oxidized and untreated CMK, which was unexpected. X-ray absorption spectroscopy (XAS) showed that the Pu(VI) was reduced to Pu(IV) at both CMK surfaces, and control experiments showed that the carbon played an essential role in the reduction. The interesting results obtained with CMK prompted further investigation, reported here, of actinide and lanthanide interactions with more pristine, robust and highly ordered OMCs.

In this paper we present the results of Pu sorption/desorption tests with FDU-16-type (**F**u**d**an **U**niversity, synthesized by evaporation-induced organic-organic self-assembly) and C-CS-type (**c**arbon from **c**arbon-**s**ilica nanocomposites, synthesized by evaporation-induced organic-inorganic co-assembly) OMCs, and their oxidized counterparts. Based on those results, more extensive batch sorption studies with C-CS and oxidized C-CS-COOH in contact with Pu(VI) and Eu(III) solutions, as well as XAS and TEM analysis of Pu-carbon samples were performed to investigate the sorption mechanism. Compared to the nanocast CMK-type carbons studied for Pu uptake previously[42], the difference in surface chemistry between C-CS and C-CS-COOH is far more distinct than the difference between CMK and nitric-acid-treated CMK. Thus the Pu experiments in the present work should resolve the ambiguity in our previous work regarding the role of oxidation of the carbon surface in the Pu sorption reaction. The sorption studies with Eu add further insight by demonstrating the behavior of these OMCs toward simple hard cations.

2. Materials and methods

2.1 Chemicals and Carbon Materials

Triblock copolymer Pluronic F127 (Mw = 12,600, PEO106PPO70PEO106) was purchased from Acros Corp. Tetraethoxysilane (TEOS), phenol, formaldehyde solution (37 wt %), hydrochloric acid (HCl), sodium hydroxide (NaOH), ammonium persulfate [$(NH_4)_2S_2O_8$, APS], sulfuric acid (H_2SO_4) and ethanol were purchased from Shanghai Chemical Corp. All chemicals were used as received without any further purification. The ordered mesoporous carbons FDU-16[43] and C-CS[44] were prepared by using Pluronic F127 as a template and phenolic resin with low molecular weight as a carbon precursor, and carbonizing at 900° C according to previous reports. The detailed synthesis procedures are provided in the supporting information. The surface oxidized mesoporous carbons denoted as FDU-16-COOH and C-CS -COOH were prepared by treating their parent carbons of FDU-16 and C-CS under a wet oxidation condition with acidic APS solution[45].

2.2 Characterization of carbon powders

Small-angle X-ray scattering (SAXS) measurements were taken on a Bruker Nanostar U small-angle X-ray scattering system with Cu Kα radiation (40 kV, 35 mA). Transmission electron microscopy (TEM) images were taken by a JEOL JEM2011F microscope operated at 200 kV. The samples for TEM measurements were suspended in ethanol and dropped onto holey carbon films supported on a Cu grid. Nitrogen adsorption/desorption isotherms were measured with a Micromeritics Tristar 3020 analyzer at -196 °C. Before the measurements, samples were degassed in vacuum at 180 °C for at least 6 h. The surface areas were calculated using the Brunauer–Emmett–Teller (BET) method. Pore size distributions were obtained based on the adsorption branch of the isotherm with the Barrett–Joyner–Halenda (BJH) method. The total pore volume was estimated from the adsorbed amount at p/p_0 of 0.995. The micropore volume and micropore surface area were calculated from the t-plot method. The particle sizes and morphologies of the four carbon powders were observed by scanning electron microscopy (SEM) using a JEOL field emission SEM (JEOL PC-SEM 6340 software) set to 5.0 kV and a 6.0 mm working distance. Fourier transform infrared (FTIR) spectra were collected on Nicolet Fourier spectrophotometer from 4000 to 400 cm^{-1} using KBr pellets of the solid samples. The C, H, N and O contents of the samples were measured on a Vario EL III elemental analyzer. Thermogravimetric analysis (TGA) was conducted on a Mettler Toledo TGA/SDTA851 analyzer from 25 to 900 °C under N_2 with a ramp rate of 5 °C min^{-1}. The relative points of zero charge (PZC) of the OMCs were measured using a modified powder addition method,[46] with a solid-to-liquid ratio of 1 g/L.

2.3 Preparation of radionuclide stock solutions

All manipulation of Pu was performed in a negative pressure glovebox, in air. All Vis-NIR absorbance spectra were acquired using an OceanOptics S2000 fiber-optic spectrometer. The ^{239}Pu(VI) stock solution was prepared from PuO_2 powder as previously described,[42] and analyzed by gamma and alpha spectroscopy, liquid scintillation counting (LSC), and Vis-NIR absorbance spectroscopy. The absorbance spectrum of the final solution indicated the presence of only PuO_2^{2+}. Because of the slow self-reduction of ^{239}Pu that occurs in aqueous solutions,[47, 48] fresh diluted ^{239}Pu(VI) stock solutions were prepared in 1-2 M $HClO_4$ each week for batch experiments.

Europium stock solutions (1.25 ± 0.08 mM Eu, and higher concentrations) were prepared by weighing $EuCl_3.6H_2O$ (Aldrich, 99.99%) and dissolving in 0.1 M HCl (Fluka analytical grade HCl, diluted in 18.2 MΩcm doubly distilled water). The ^{152}Eu solution in 0.1 M HCl was purchased from Eckert & Ziegler and used to spike the stock solutions to reach a total specific activity of 1000 ± 100 Bq/µL.

2.4 Batch contact experiments

All solutions were prepared with 18.2 MΩcm doubly distilled (Milli-Q) water and ACS reagent grade or better reagents. Batch samples were prepared in polypropylene tubes that had been leached with 10% HCl, followed by Milli-Q water and thorough rinsing. Samples of pH-adjusted 0.1 M $NaClO_4$ or NaCl with OMC powders were generally prepared one day before addition of radionuclides, with a liquid-to-solid ratio of 1000 ± 50 mL/g. All experiments were performed under air, at room temperature. Eppendorf micropipettors were used to add known amounts of stock solution, and the pH was quickly adjusted to the desired value with small volumes of NaOH, $HClO_4$ or HCl. The samples were mechanically rocked for the desired length of time. The phases were separated as described in the supporting information, and the concentration of Pu or Eu left in the liquid phase was measured by LSC or gamma spectroscopy. Control samples with no solid sorbent were prepared to test the radionuclide solubility, as well as sorption to vial walls and filters (when filters were used).

Plutonium aliquots were counted for 30 minutes each with a Wallac 1414 LSC operating in *α/β* discrimination mode to determine the concentration of Pu remaining in solution. Aliquots from Eu samples were counted for at least 2 hours each with a high purity germanium detector (Ortec). The 344 keV gamma peak from ^{152}Eu was used to quantify the remaining Eu in solution. Great care was taken to ensure consistent counting geometry. All liquid aliquots were measured in duplicate and average values are reported. Experiments were performed at least twice to examine reproducibility and data from duplicate experiments were not averaged. Uncertainties at the 1σ confidence level of measured concentrations incorporate an estimated 2.5% pipetting uncertainty, the standard error between duplicate measurements, and 1σ from counting statistics. The error bars on percent sorption represent 2σ by using a worst-case method with upper limits for initial and final concentrations (c) of c+2σ, and lower limits of c-2σ.

2.5 Plutonium XAS measurements

The XAS samples were prepared in a similar manner to the batch sorption samples described above. 60 ± 3 mg $^{239}Pu(VI)$ per gram carbon was loaded on to C-CS samples with 1020 ± 10 mL 0.1 M $NaClO_4$ solution (245 ± 13 μM Pu) per gram carbon. After 1 day of contact, LSC measurements determined that 99.9 ± 0.5 % of the Pu was associated with the C-CS-COOH solid phase, and 97.8 ± 0.6 % of the Pu was associated with the C-CS solid phase. Packaging and measurement of XAS samples was performed using the method of Hu et al.[49] The carbon samples were loaded as wet pastes into Kapton tubes and triply contained in specialized sample holders before shipment to the Stanford Synchrotron Radiation Light source (SSRL). The production and measurement of Pu(IV), Pu(V), and Pu(VI) solution spectra used for the XANES analysis were published previously.[50] Pu L_{III}-edge XAS spectra were collected at SSRL on beamline 11-2, with samples held at 30 ± 2 K, in fluorescence mode using a 100-

element germanium detector. The XAS data were collected, processed and analyzed as described previously,[42] and further details are provided in the supporting information.

2.6 TEM analysis of plutonium on OMC

Batch samples for TEM analysis were prepared identically to the XAS samples described above, except that the carbon powders were ground with a mortar and pestle before sample preparation. After 1 day of contact, LSC measurements determined that 99.7 ± 0.3 % of the Pu was with the C-CS-COOH solid phase, and 95.0 ± 1.2 % of the Pu was associated with the C-CS solid phase. The solid phase was allowed to settle, and the bulk liquid phase was removed. The solid phase was washed 10 times by adding 10^{-4} M HCl, shaking for 1 minute, centrifuging for 10 minutes at 7000 rpm, and then decanting the liquid phase. LSC analysis of the supernatants determined that over 98% of the total Pu added remained on the solid phase in the C-CS-COOH sample, and over 88% remained associated with the C-CS. The samples were shipped as approximately 0.3 g/L slurries in 10^{-4} M HCl to Lawrence Livermore National Laboratory (LLNL), where 10 µL aliquots were drop-cast onto lacey formvar/carbon coated Cu TEM grids. The micrographs were collected with a Philips CM300 FEG TEM operating at 300 kV. The *in-situ* elemental analysis was performed by X-ray energy dispersive spectroscopy (EDS) with an Oxford detector under the TEM. Several grids were prepared and analyzed with each sample to ensure that micrographs were representative of the bulk sample.

3. Results and discussion

3.1 Synthesis and characterization of OMCs

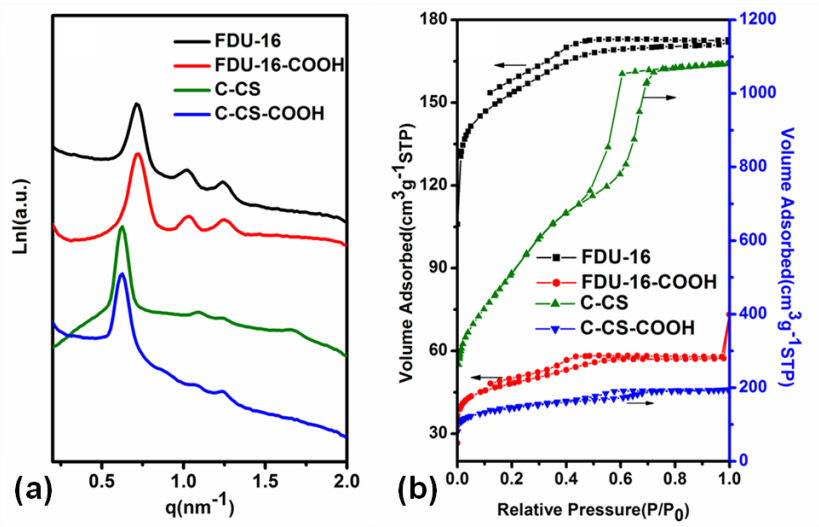

Figure 1. SAXS patterns (a) and N_2 adsorption isotherms (b) of FDU-16, FDU-16-COOH, C-CS, and C-CS-COOH mesoporous carbon powders.

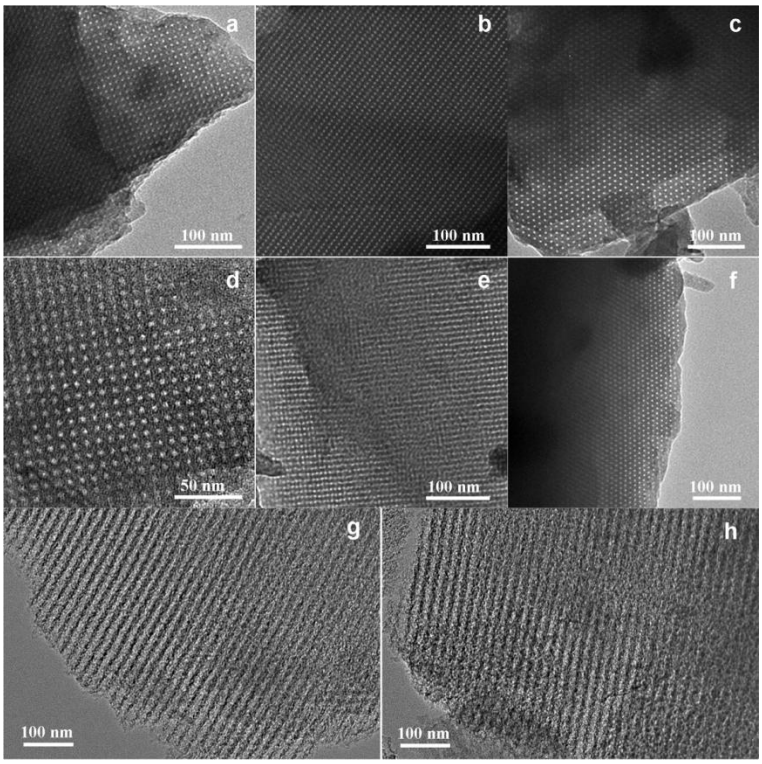

Figure 2. TEM images of FDU-16 (a,b,c), FDU-16-COOH (d,e,f), viewed along the [100] (a, d), [110] (b, e), and [111] (c, f) directions; and C-CS (g) and C-CS-COOH (h) viewed along the [110] direction.

The OMC FDU-16 was synthesized by evaporation-induced organic-organic self assembly.[43] Its SAXS pattern (Figure 1a) shows three well-resolved scattering peaks that can be indexed to the 110, 200 and 211 diffractions of a highly ordered three-dimensional (3D) cubic *Im3m* mesostructure. After treatment with acidic APS solution at 60 °C for 12 h, the SAXS pattern (Figure 1a) of FDU-16-COOH shows similar diffractions to that of FDU-16, indicating that the mesostructural regularity was retained. This is further confirmed by TEM images that show the 3D cubic mesostructure in large domains of FDU-16 (Figure 2a,b,c) and FDU-16-COOH (Figure 2d,e,f). The OMC C-CS was synthesized by etching the silica component from a carbon-silica nanocomposite produced by the evaporation-induced triconstituent co-assembly method.[44] The SAXS pattern (Figure 1a) shows four resolved diffraction peaks, which can be indexed to 10, 11, 20 and 21 planes of a 2-D hexagonal mesostructure (space group *p6m*). After oxidation treatment by APS, the C-CS-COOH maintained the ordered mesostructure as evidenced by SAXS (Figure 1a) and TEM images (Figure 2g,h).

Table 1: Physical properties of OMCs derived from N_2 adsorption, SAXS, and TEM.

OMC	Unit Cell Parameter (nm)	BET Surface Area (m^2/g)	Micropore area (m^2/g)	BJH Pore Diameter (nm)	Pore Volume (cm^3/g)	Micropore Volume (cm^3/g)	Meso-structure
C-CS	11.6	1817	199	2.1/6.0	1.67	0.08	*p6m*
C-CS-COOH	11.6	521	310	2.1/6.2	0.30	0.13	*p6m*
FDU-16	12.4	564	424	2.7	0.27	0.17	*Im3m*
FDU-16-COOH	12.4	176	122	3.3	0.11	0.05	*Im3m*

Table 2: Chemical properties of OMC derived from elemental analysis, powder addition and TG data.

Sample	PZC (pH)	Carboxyl (mmol/g)	Phenol (mmol/g)	C/H/N/O wt %
C-CS	7.3 ± 0.4	0.17	0.19	86.9/3.6/0.1/9.1
C-CS-COOH	2.8 ± 0.1	1.89	2.13	56.2/4.1/0.2/39.5
FDU-16	7.1± 0.1	0.28	0.26	91.7/4.3/0.4/2.7
FDU-16-COOH	3.1 ± 0.1	0.89	0.57	84.6/3.6/0.4/11.4

N_2 adsorption isotherms (Figure 1b) of FDU-16, C-CS and their oxidized counterparts all show type-IV curves, indicating typical mesoporous materials. Table 1 summarizes the physical properties of these four mesoporous carbons. Clearly, C-CS has a much higher surface area and pore volume than the FDU-16 due to the secondary pore network inside the walls of the primary mesostructure.[44] The surface areas and total pore volumes of both the APS treated samples are significantly lower than the untreated samples. The oxidation occurs preferentially in the smallest pores, leaving the micropores blocked, while degradation of carbon layers give mesopores that are slightly larger than those of the pristine carbons (Figure S1).[45] SEM images of the carbon powders (Figure S2) showed that the FDU-16 particles are significantly larger (~10 μm - 1 mm) than the C-CS particles (~1 - 100 μm). Particle size has little effect on the BET surface areas of OMCs, as most of the surface area is internal, but may alter sorption kinetics by limiting the rate of diffusion of aqueous species into the pores.

FTIR spectra (Figure S3) show a new band at 1721 cm^{-1} attributed to the carbonyl stretch of non-aromatic carboxyl groups[45, 51, 52] appear for both FDU-16-COOH and C-CS-COOH with treatment by APS. A strong band at 1590 cm^{-1} also occurs, which can be attributed to symmetric COO- vibration and/or aromatic ring stretching coupled to highly conjugated keto groups.[45] The intensity of these bands are most evident in the FTIR spectrum of C-CS-COOH, which has the highest concentration of

surface groups measured by TGA. Table 2 summarizes some chemical properties of the OMC surfaces, as determined by elemental analysis, TGA and powder addition. The carbon content decreased while the H and O content increased dramatically after the treatment with APS (Table 2), indicating successful functionalization. The densities of surface oxides were determined by TGA measurement according to a previous report.[45] The density of carboxylic groups calculated based on the weight loss between 150 and 280 °C is 0.89 and 1.89 mmol/g for FDU-16-COOH and C-CS-COOH, respectively. This is much higher than that of the untreated FDU-16 and C-CS. A similar phenomenon is also observed for the density of phenolic groups, which was calculated based on the weight loss from 280-350 °C. Furthermore, the high concentration of carboxyl groups on the oxidized materials leads to much lower PZCs in these materials, compared to the near-neutral PZCs of the pristine C-CS and FDU-16 carbons.[53, 54] The plots of ΔpH (pH_{final} - $pH_{initial}$) vs. $pH_{initial}$ from powder addition experiments (Figure S4) were linear within the initial pH range 5 to 9 for the untreated carbons and 3 to 10 for the oxidized carbons ($R^2 \geq 0.99$).

3.2 Oxidation state of Pu in solutions

The Eu solutions are stable in the trivalent oxidation state, as highly reducing conditions would be needed for a stable divalent state to exist.[55] However, ^{239}Pu(VI) undergoes auto-reduction to Pu(V) under most aqueous conditions.[5, 47, 48] As discussed in our previous work,[42] it is expected that at the time that LSC measurements were undertaken the solutions would be a mixture of Pu(VI), Pu(V), and a very small amount (< 10 %) of Pu(IV) colloid. Control samples of 250 ± 17 μM Pu, added as Pu(VI), in 0.1 M $HClO_4$ adjusted to pH 4, were monitored by Vis-NIR spectroscopy to estimate how much Pu(VI) would remain in concentrated solutions after various amounts of time, without the carbon solid.[42] After one day, the Pu(VI) peak near 830 nm in the spectra of these control samples showed approximately 80 % of its original intensity. This was further reduced to about 67% after 2 days, and 40 % after one week. LSC monitoring showed that 94 ± 7 % of Pu in these control samples remained in the solution phase after 2 days.

3.3 Plutonium and europium sorption and desorption to OMCs as a function of solution pH

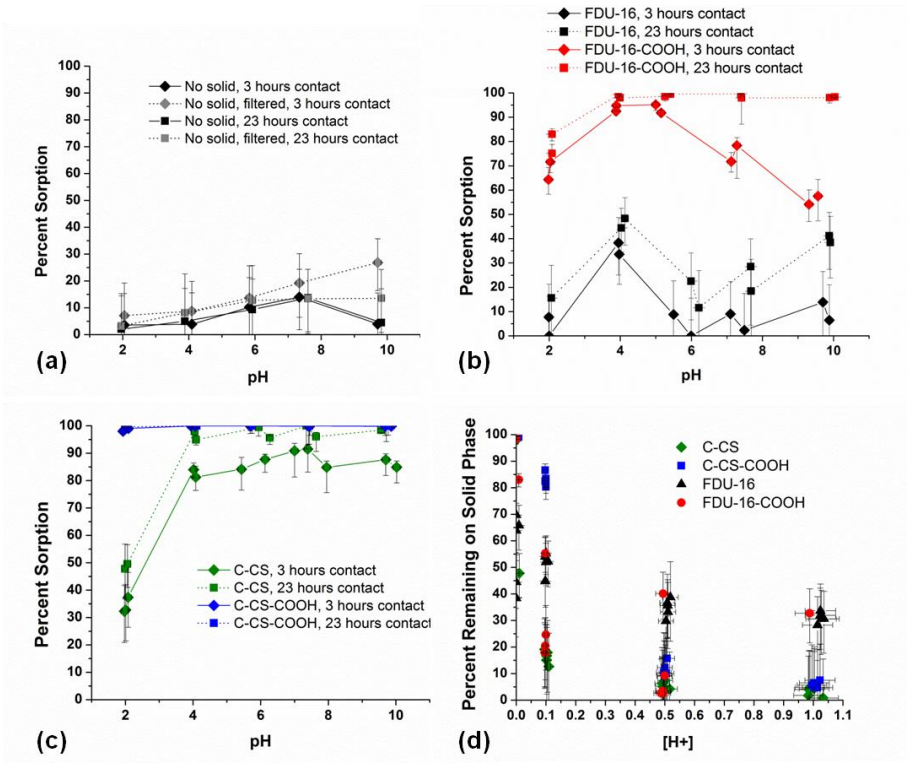

Figure 3. Percent Pu sorption vs. pH for control samples of 0.1 M $NaClO_4$ and 10 ± 1 µM Pu(VI) solution (a), samples of FDU-16 and FDU-16-COOH OMC powders (b), and samples of C-CS and C-CS-COOH OMC powders (c) measured after 3 hours and 23 hours. Lines are only to guide the eye. Panel (d) shows the total percentage of Pu remaining on the solid phase vs. total acid concentration as $HClO_4$ was incrementally added the batch sorption samples and allowed 24 hours desorption time.

The Pu affinities of all four OMC powders were tested in batch contact experiments with 10 ± 1 µM Pu(VI) in a 0.1 M $NaClO_4$ matrix at pH values between 1 and 10. Figure 3 shows percent sorption vs. pH for those samples, measured after 3 and 23 hours. No significant sorption or precipitation of Pu in control samples (Figure 3a) occurred in solutions below pH 6, and a small amount seemed to have precipitated in the higher pH solutions. Therefore any loss of Pu from the solution phase greater than 25% in carbon samples can be attributed to sorption to the carbons. There is a large range of sorption behavior among the OMC samples. Pristine FDU-16 (Figure 3b) is not an effective sorbent material for Pu, while oxidized FDU-16-COOH showed high uptake from solutions of pH 4 and greater. However, the large particle size and relatively low surface area likely slowed the sorption process, and complete sorption was only observed after 23 hours. The higher surface-area C-CS-type OMCs show high Pu uptake from solutions over a wide pH range. In solutions with pH 2-10, near 100% sorption to C-CS-COOH was achieved within 3 hours of contact time (see Figure 3c). Greater than 90% Pu sorption to the pristine C-CS OMC occurred more slowly, but only at pH values ≥ 4.

It is important for most applications that target species can be removed after binding to the surface. To test desorption, $HClO_4$ was added incrementally to the samples, allowing 24 ± 1 hours desorption time at each acidity. Figure 3d shows that most of the adsorbed Pu was removed from C-CS and FDU-16-COOH in 0.1 M acid, but about 80-90% of the Pu in C-CS-COOH

samples remained on the solid phase. This is likely due to the very high concentration of negatively charged functional groups on the C-CS-COOH, even in 0.1 M acid (pH 1). Over 90% of Pu was stripped from C-CS-COOH with 0.5 M $HClO_4$. Only the FDU-16 samples and the pH 10 sample of FDU-16-COOH retained over 30 % of the Pu in 1 M acid, indicating Pu may have precipitated in those samples.

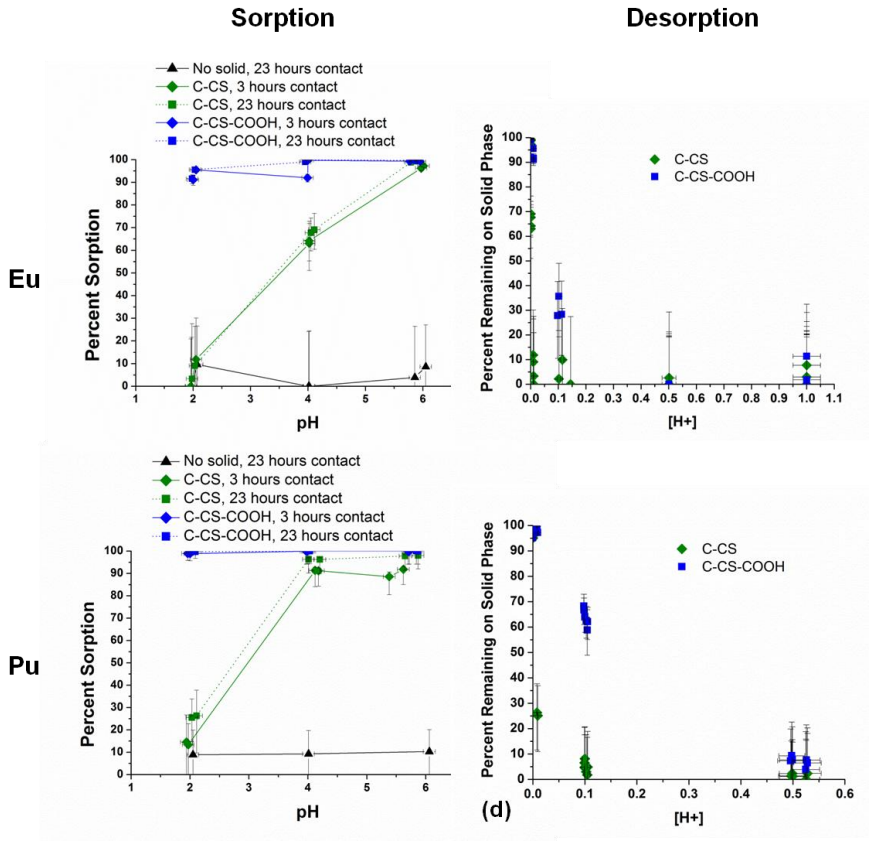

Figure 4. Percent sorption vs. pH after 23 hours for samples of 0.1 M NaCl and 10 ± 1 µM Eu(III) (a) or Pu(VI) (c) at different pH values and C-CS OMC powders. Lines are added to guide the eye. Panels b and d show the total percentage of Eu or Pu remaining on the solid phase vs. total acid concentration as HCl was incrementally added to the batch sorption samples and allowed 24 hours desorption time.

Because C-CS type OMCs were more effectively oxidized by APS, and demonstrated superior Pu sorption behavior to the FDU-16 type, subsequent experiments investigated the interactions of Pu(VI) and Eu(III) with pristine C-CS and oxidized C-CS-COOH. Eu sorption to unoxidized OMCs should be pH-dependent and may be less favorable than sorption of Pu, as Eu(III) is expected to only interact electrostatically with deprotonated surface groups. Uptake of 10 ± 1 µM Eu by the C-CS carbons was measured from 0.1 M NaCl solutions with pH values 2, 4 and 6 (Figure 4a). Solutions with higher pH values were not investigated to avoid insoluble Eu hydrolysis products in solution, and in control (no solid) samples less than 20% loss of Eu to the vial was observed in all tested pH conditions. For both materials, no significant difference in Eu sorption was observed after 23 hours compared to 3 hours contact. In pH 4 solution 70 ± 7 % Eu sorption to C-CS was observed (Figure 4a), compared to 96

± 6 % Pu (Figure 4c), indicating that the untreated OMC surface has more affinity for Pu than for Eu. Figure 4c shows that the Pu sorption to the OMCs in 0.1 M NaCl is similar to that in 0.1 M $NaClO_4$ (Figure 3c).

The reversibility of sorption upon incremental addition of HCl to Eu and Pu samples is shown in Figure 4b and d. As with Pu sorption, Eu sorption to C-CS is reversible in 0.1 M HCl (Figure 4b). Approximately 30% of the total Eu was retained by C-CS-COOH in 0.1 M HCl, but was removed by increasing the acidity to 0.5 M. Figure 4d shows that 60-70% of the total Pu was retained by C-CS-COOH in 0.1 M HCl, indicating that the Pu is more strongly bound to the oxidized surface than Eu. The Pu desorption trends (Figure 4d) are similar to those observed with $HClO_4$ (figure 3d), with slightly less Pu being retained by the C-CS and C-CS-COOH in 0.1 M HCl than in 0.1 M $HClO_4$.

3.4 Sorption kinetics

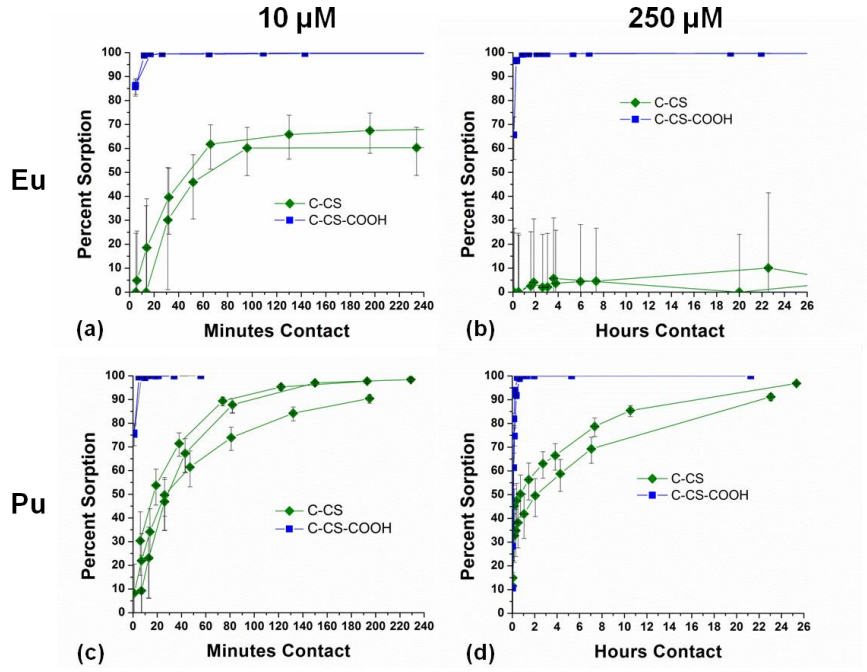

Figure 5. Percent sorption vs. contact time for batch C-CS samples with approximately 1000 mL/g of pH 4 0.1 M NaCl 10 ± 1 µM Eu solution (a), pH 4 0.1 M NaCl 250 ± 15 µM Eu solution (b), pH 4 0.1 M $NaClO_4$ 10 ± 1 µM Pu solution (c), and pH 4 0.13 M $NaClO_4$ 250 ± 17 µM Pu solution (d). Lines are added to guide the eye along data points taken from the same sample.

Figure 5 shows the sorption vs. contact time for samples of C-CS and C-CS-COOH in pH 4 solutions of: 0.1 M NaCl 10 ± 1 µM Eu (a), 0.1 M NaCl 250 ± 15 µM Eu (b), 0.1 M $NaClO_4$ 10 ± 1 µM Pu (c) and 0.1 M $NaClO_4$ 250 ± 17 µM Pu (d). In the lower concentration samples, quantitative Pu and Eu sorption to C-CS-COOH occurred immediately upon adjustment of the solution to pH 4 (the first two data points in each set were taken while the solution pH was still about 1.5-2.8). The pristine C-CS carbon reached a steady-state with Eu within 100 minutes (Figure 5a), but took about 180 minutes for maximum Pu sorption (Figure 5c). Pu uptake by pristine C-CS was slower than the uptake by both untreated and oxidized CMK in our previous work [42]

and sorption to C-CS-COOH was faster. The trends observed in these four OMCs show that the sorption rate increases with the concentration of oxygen-containing functional groups in the sample, and the mechanism appears to be controlled by surface chemistry. All of the kinetic data from batch Eu and Pu sorption samples fit well to the pseudo-second-order rate model described in the supplemental information, which indicates that the sorption mechanism is second-order with respect to the carbon.[41, 56]

Our previous kinetic data collected on batch 250 µM Pu samples of untreated and oxidized CMK suggested that the carboxyl and other surface groups in both samples were saturated, and further sorption occurred by a different mechanism.[42] Because the concentration of carboxyl groups in the C-CS-COOH is far greater than in those CMK materials, samples of C-CS and C-CS-COOH with high Pu concentrations were expected to yield very different results. Figure 5d shows untreated C-CS samples took over 23 hours to reach maximum sorption, like the CMK samples. However, complete Pu sorption to C-CS-COOH occurs within 30-40 minutes under these conditions. Approximately 0.25 mmol Pu per g carbon was loaded in these samples, so the surface carboxyl groups in the C-CS are saturated, and in the C-CS-COOH there is still an excess of surface groups. These results show further evidence that sorption occurs preferably via complexation by deprotonated carboxyl groups, and when no surface groups are available an alternate binding mechanism is employed for increased Pu uptake. No significant Eu uptake from 250 µM Eu samples was observed to C-CS, while quantitative Eu uptake to C-CS-COOH occurred within 1 hour (Figure 5b). There were no further changes in Eu concentration in these samples over the course of 3 days. Hence, C-CS-COOH is a fast and effective scavenger of both actinide and lanthanide cations, while the high sortion to C-CS is unique to Pu.

3.5 Effect of ionic strength on Pu sorption

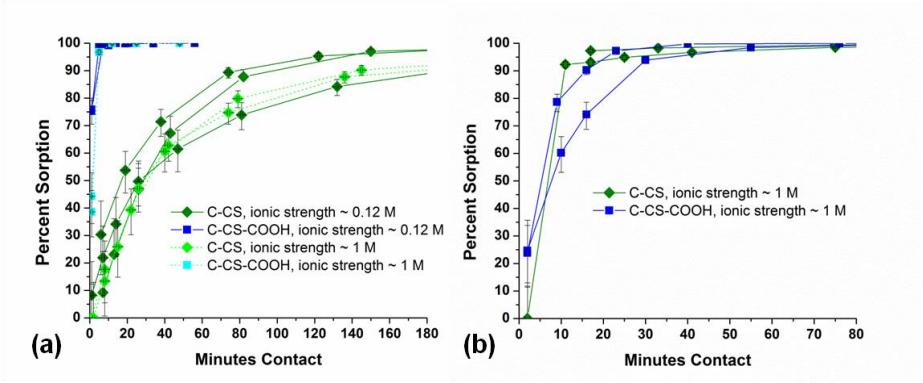

Figure 6. Percent sorption vs. minutes contact for C-CS carbon powders with 10 µM Pu, pH 4 $NaClO_4$ solutions of different ionic strengths (a), and 250 µM Pu, pH 4 $NaClO_4$ solutions with ionic strength of approximately 1 M (b). Lines are added to guide the eye along data points from the same sample.

Ionic strength can strongly influence sorption if outer-sphere complexation or physisorption is involved. If the binding mechanism is due to chemisorption, or inner-sphere complexation, then the uptake should be independent of ionic strength.[57] The effect of ionic strength on Pu sorption to C-CS and C-CS-COOH was tested in the non-complexing $NaClO_4$ medium at pH 4 with

10-15 µM Pu (Figure S6). The ionic strength in this range did not significantly affect the sorption of Pu to either C-CS or C-CS-COOH. These results were expected for C-CS-COOH, and indicate Pu is bound via chemisorption. The effect of ionic strength on the Pu sorption kinetics of these two materials was tested at two Pu concentrations, and proved to be negligible in samples of 10 µM Pu (Figure 6a), and all samples of C-CS-COOH. Figure 6b shows the sorption time for samples with 250 µM Pu, perchlorate solutions with ionic strengths near 1 M. The time required for complete uptake to C-CS-COOH was the same as with lower ionic strength (see Figure 5d), but complete sorption to C-CS occurred much faster, within 20 minutes instead of 24 hours. This unexpected result again suggests that Pu sorption to C-CS at high Pu concentrations occurs by an alternate mechanism. Considering that past Pu XAS data on CMK samples showed that Pu(VI) and Pu(V) were reduced to Pu (IV) at the carbon surface,[42] we hypothesized that the high Pu sorption to unoxidized C-CS is either surface precipitation or adsorption of Pu(IV) intrinsic colloids. The increased rate of Pu sorption to C-CS that was observed at higher ionic strength could actually be an increase in the rate of Pu colloid formation. However, no clear trend was observed when the batch kinetic experiment was repeated at intermediate ionic strengths around 0.3, 0.5 and 0.7 M (Figure S7), the Pu sorption was slow in all of those samples. The higher ionic strength had little to no effect on Eu sorption in samples of pH 4, 1 M $NaClO_4$, 250 ± 15 µM Eu (Figure S8).

3.9 Eu sorption capacities of C-CS and C-CS-COOH

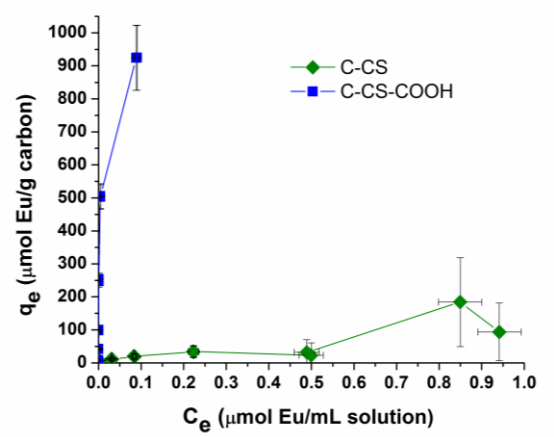

Figure 7. Eu(III) sorption isotherms for C-CS samples with approximately 1000 mL/g of pH 4 0.1 M NaCl solutions with Eu concentrations ranging from 10 µM to 1 mM. Lines are added to guide the eye, error bars represent 1σ.

The Eu uptake capacities of C-CS and C-CS-COOH were estimated by preparing duplicate samples of 1000 mL/g pH 4 0.1 M NaCl solutions with total Eu concentrations 10 µM, 50 µM, 100 µM, 250 µM, 500 µM, and 1 mM, and measuring the solution concentration of Eu after 2 days of contact. The isotherm data are plotted in Figure 7, and show that the Eu binding sites on C-CS-COOH are not saturated with 900 µmol Eu per g C-CS-COOH, while the Eu capacity of C-CS is limited to under 100 µmol/g. The C-CS-COOH Eu sorption isotherm data fit very well to the Langmuir model (described in supporting information), implying homogenous chemisorption. The derived monolayer sorption capacity is 0.91 mmol/g (138 mg/g), which is far greater than previously reported Eu capacities of activated carbons[7, 8] or carbon nanotubes,[24, 25] and comparable to the Eu capacities

reported for graphene oxide in pH 4.5-5 solutions.[28, 29] Furthermore, the Eu sorption capacity of C-CS-COOH is far greater than those reported for several other adsorbents, such as minerals and zeolites.[28] The Pu uptake capacities cannot be measured with sorption isotherms, because of solubility limitations and lack of equilibrium in the samples. Both C-CS and C-CS-COOH removed the entire 60 ± 3 mg Pu from pH 4 solutions (Figure 5d), and the true uptake capacities are likely much greater.

3.6 TEM and XAS analysis of Pu sorbed to C-CS-type OMCs

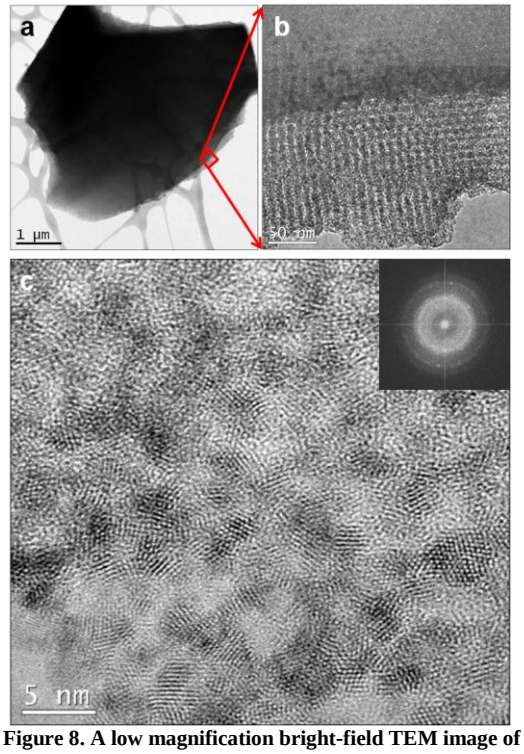

Figure 8. A low magnification bright-field TEM image of a C-CS mesoporous carbon particle (a), a magnified image from the edge of the C-CS particle (b), and further magnified HR-TEM image (c). Nano-particles with a primary size of ~3nm in diameter can be identified. The corresponding Fourier transform (FFT) pattern (c inset) matches the structure of fcc PuO_2.

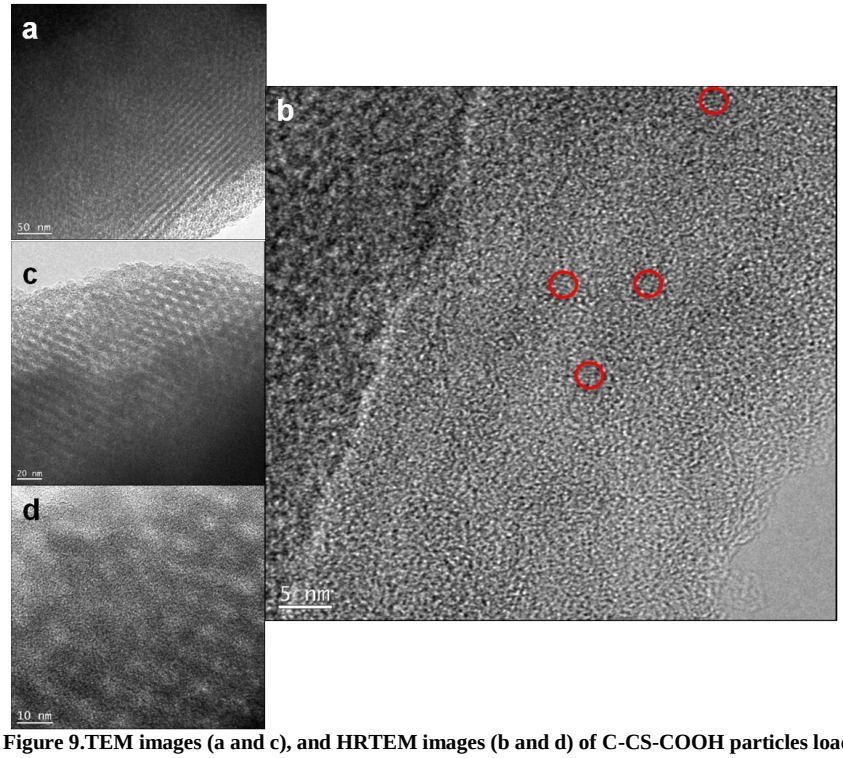

Figure 9.TEM images (a and c), and HRTEM images (b and d) of C-CS-COOH particles loaded with Pu. No crystalline PuO_2 particles were identified, but some local ordered clusters can be identified, as marked by circles (b).

Samples of C-CS and C-CS-COOH were prepared under identical conditions (1000 mL pH 4, 245 ± 13 µM Pu, 0.1 M $NaClO_4$ solution per g carbon) for analysis by TEM and XAS, in order to characterize the Pu associated with the carbon surfaces. Figure 8 shows a low-magnification TEM image of a C-CS particle loaded with Pu (a), and magnified TEM (b) and HRTEM (c) images of the edge of the particle. HRTEM images of all Pu-loaded C-CS particles examined showed a high concentration of crystalline nanoparticles on the surface, about 3 nm in diameter (see Figure 8c). The Fourier transforms (FFTs) shown in the inset correspond with the face centered cubic (fcc) structure of crystalline PuO_2. The size of the crystals is about the same as the secondary mesopore network in C-CS, but there is no evidence that this is more than coincidence. Pu oxide nanoparticles of similar size were observed by Romanchuk et al.[58] via HRTEM on hematite that had Pu(VI) added to it, and by Powell et al.[59] with incremental addition of Pu(IV) to quartz and goethite. In that work, the nanocolloids formed on quartz and in solution were fcc PuO_2, but the crystals formed on the goethite surface epitaxially adopted the bcc Pu_4O_7 structure. In the present work, no such epitaxial distortion was expected due to the amorphous nature of the carbon, and it is not clear whether these PuO_2 nanocrystals grew onto the surface of C-CS, or were formed in solution and then adsorbed strongly to the surface. In either case, the carbon must have first reduced Pu(VI) and Pu(V) to Pu(IV). The PuO_2 nanocrystals are strongly associated with the C-CS particles, as the 10 cycles of rinsing did not remove them, and they were not observed on the TEM grids apart from the C-CS particles. Figure 9 shows TEM images (a, c) and HRTEM images (b, d) of C-CS-COOH particles loaded with Pu. In all of the HRTEM images of C-CS-COOH samples, no crystalline PuO_2 particles were observed, even though strong Pu peaks were identified in the

corresponding X-ray EDS spectra (Figure S10b). A few tiny clusters of local order were observed on some C-CS-COOH particles (circled in Figure 9b), which may or may not contain Pu. The majority of the Pu associated with the C-CS-COOH is amorphous, and presumably complexed by carboxyl and other surface groups. The TEM images provided direct evidence that Pu sorbs to pristine carbon surfaces in the form of nanocolloids, while monomeric Pu species and/or small disordered clusters sorb to highly oxidized surfaces. It should be noted that the X-ray EDS spectra from the C-CS particles (example in Figure S10a) indicated the presence of only C, O, and Pu, but the spectra from some of the C-CS-COOH particles showed traces of Al, Fe, or Si as well (Figure S10b). The trace Si seems to be left over from the synthesis, but the Fe and Al were not detected by elemental analysis of the bulk C-CS-COOH sample. None of the contaminants seemed to be associated with the Pu on the grids, and repeated batch experiments after dialysis of the C-CS-COOH indicated no change in Pu sorption behavior (Figure S11).

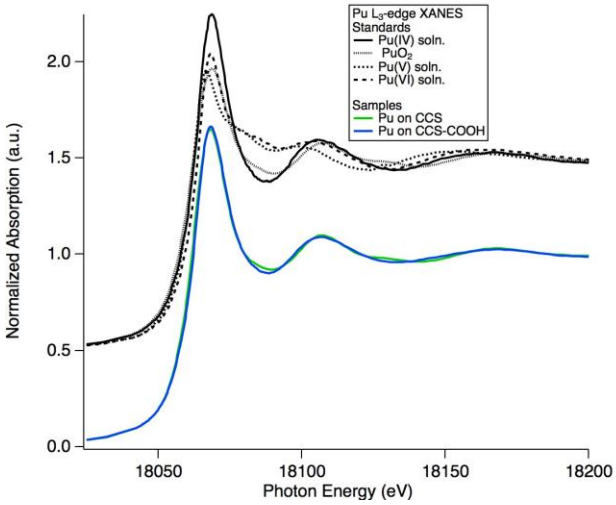

Figure 10. XANES spectra of the Pu on C-CS samples, and associated Pu reference spectra (offset for clarity) used in XANES fitting. The spectra of both samples lack the plutonyl shoulder seen in Pu(V) and Pu(VI) spectra.

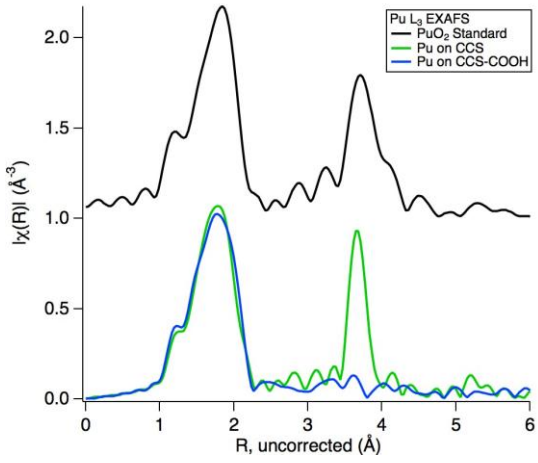

Figure 11. Fourier transform magnitude of the EXAFS from C-CS samples, and PuO_2 (offset) for comparison. The difference in widths of the Pu-Pu scattering peak between the PuO_2 and the untreated C-CS sample is an artifact of the shorter k-space range available for the Fourier transform of the PuO_2 standard.

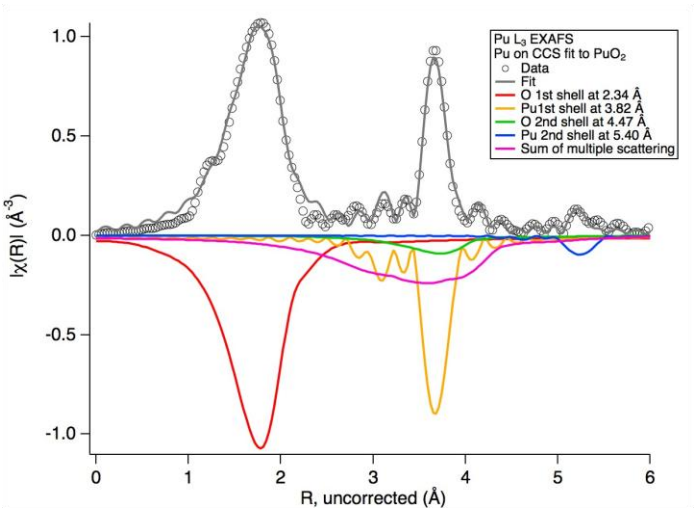

Figure 12. Fitting of the Pu EXAFS in the C-CS sample to the PuO_2 crystal structure. Scattering shells have been reflected about the x-axis for clarity, and the 8 weak multiple scattering paths used in the fit have been summed as well. The first 11 scattering paths, as well as the 2nd shell Pu path have been used in the fit. The R-factor of the fit to the C-CS sample was 0.0297, and for the C-CS-COOH sample it was 0.0995.

Table 3: Summary of EXAFS path fitting results, where fitting a total of 12 paths each for the PuO_2 standard and the sample were refined simultaneously using 10 variables over approximately 70 independent points. The E_0 shift for the C-CS sample was 2.6 ± 0.3 eV, and 2.6 ± 0.6 eV for the C-CS-COOH sample.

Sample	Scattering Shell	R (Å)	No. of Atoms	Debye-Waller Factor (Å^2)
Pu-C-CS	Oxygen	2.31 ± 0.03	7.8 ± 1.0	0.0086 ± 0.0009
	Plutonium	3.81 ± 0.01	6.2 ± 1.0	0.0036 ± 0.0003
	Plutonium	5.39 ± 0.01	1.7 ± 0.9	0.0036 ± 0.0003
Pu-C-CS-COOH	Oxygen	2.33 ± 0.01	9.1 ± 2.0	0.011 ± 0.0017
	Plutonium	3.81 ± 0.02	0.3 ± 0.3	0.0016 ± 0.0014
	Plutonium	5.39 ± 0.02	0.1 ± 0.1	0.0016 ± 0.0014

Pu L_{III}-edge XANES spectra (Figure 10) collected from C-CS and C-CS-COOH samples show little of the characteristic plutonyl shoulder that would be expected if significant amounts of Pu(V) or Pu(VI) were present in the samples. Linear combination analysis (LCA) results of the XANES spectra confirm that all of the Pu in both samples is tetravalent. Without the carbon solids, the Pu solution would contain a mixture of Pu(VI) and Pu(V) at the time of measurement,[42] thus the XANES results show that both C-CS and C-CS-COOH reduce Pu(VI) and Pu(V) to Pu(IV). Analysis of the EXAFS data shown in Figure 11 can confirm the presence or absence of PuO_2 particles that were observed in the C-CS TEM sample. Figure 11 shows that in the EXAFS of the C-CS-COOH sample there is little to no contribution from the first Pu-Pu scattering shell at 3.82 Å, in contrast with the C-CS sample, which shows a strong scattering feature consistent with that seen in bulk PuO_2. The EXAFS data sets from samples were fit simultaneously with the PuO_2 standard data set to a model based on PuO_2 (Figure 12 shows C-CS

fit). This technique applied to the C-CS-COOH data indicated little change in the first oxygen shell, consistent with Pu(IV), but essentially no Pu-Pu scattering that would be expected if there were any bulk PuO_2 precipitates. Table 5 summarizes the fitting parameters for the EXAFS data. The XAS data shows that although both C-CS and C-CS-COOH reduce Pu(V/VI) to Pu(IV), PuO_2 is only formed in C-CS samples. These results corroborate very well the TEM results presented above.

The batch sorption, XAS, and TEM experiments with oxidized Pu on unmodified and highly oxidized C-CS have illustrated how Pu interacts with OMCs. Both oxidized and pristine OMCs show high sorption capacities for Pu in aqueous pH 4 solutions, at least 60 mg Pu per g carbon, and both reduce Pu(V/VI) to Pu(IV). Chemisorption to carboxyl and possibly other functional groups on the surface occurs rapidly, and this prevents Pu(IV) from forming colloids in pH 4 solutions with C-CS-COOH. Once those surface binding sites are saturated, any remaining Pu(IV) forms PuO_2 nanocrystals that strongly associate with the carbon surface. Kinetic data suggest that the formation of PuO_2 nanocolloids is the rate-limiting step for Pu sorption to pristine OMCs. The batch sorption data with Eu indicate that oxidized OMCs make an effective general sorbent material for other actinide and lanthanide cations, while the high sorption to pristine OMCs may be unique to Pu, due to the reduction and subsequent formation and sorption of PuO_2 nanocrystals. This sorption is significant, as the nanocrystals otherwise form stable aqueous suspensions, and are not removed by centrifugation. Along with high surface area, the pore size distribution may be important for effective sorption of Pu nanocolloids, as similar batch experiments with commercial activated carbon, which generally contains micropores (< 2 nm), showed much lower Pu sorption.[42] The larger pores and high surface areas of mesoporous materials are ideal for sorption of large molecules and colloids. For example, C-CS type OMC recently proved to be an excellent adsorbent material for the large toxic bio-molecule microcystin-LR.[60]

4. Conclusions

Highly ordered FDU-16-type and C-CS-type OMCs were synthesized and characterized by SEM, TEM, SAXS, N_2 adsorption, elemental analysis, TGA, FTIR and PZC determination. A portion of the as-synthesized OMCs were oxidized via treatment with acidic APS, which created a high density of surface carboxyl and phenol groups. Exploratory batch experiments performed with 10 µM Pu(VI), 0.1 M $NaClO_4$ solutions of various pH conditions, showed that oxidized C-CS-COOH was the most efficient Pu scavenger, and further investigations focused on comparison of the Pu and Eu sorption interactions with pristine and oxidized C-CS-type OMCs.

Oxidized C-CS-COOH mesoporous carbon is very fast and effective scavenger of Pu and Eu. This material removes cations from aqueous solutions via chemisorption, and the monolayer sorption capacity for Eu(III) in pH 4 solution (0.91 mmol Eu per g C) is higher than those reported previously for most other carbon-based materials.[8, 24, 25] Pristine C-CS showed a low affinity for Eu, but a large capacity for Pu sorption. XAS and TEM data showed that Pu(VI/V) was reduced to the tetravalent

state by both oxidized and untreated C-CS. The oxidized C-CS-COOH complexed monomeric Pu(IV) and/or small amorphous Pu oxide clusters, preventing the formation of crystalline PuO_2 in pH 4 solution. Pristine C-CS shows high sorption affinity for PuO_2 nanocrystals (~3 nm diameter) formed at or near the carbon surface. This apparent selectivity for Pu uptake is a novel finding of pristine carbon surfaces, and could be valuable for a variety of applications involving separation or sequestration of actinides. Current sorption studies in our laboratory with Pu(IV), U(VI), and Np(V) should help clarify the roles of redox chemistry and actinyl oxygens in the actinide interactions with ordered mesoporous carbon.

Acknowledgements. The authors would like to thank Professor Peidong Yang of UC Berkeley for his help in establishing the collaboration between the Zhao group of Fudan University and the Nitsche group of UC Berkeley. The authors would like to thank Deborah Wang for her assistance with the XAS experiment. The authors would like to thank the anonymous reviewers for helping to improve the quality of this manuscript. The majority of this work was supported by the US Department of Homeland Security Academic Research Initiative (ARI) program under Grant Award Number, 2012-DN-130-NF0001-02. A part of this work was supported by the U.S Department of Energy (DOE), National Nuclear Security Administration (NNSA) through the Stewardship Science Academic Alliances Program (SSAAP) under award numbers DE-NA0001978 and DE-FG52-10NA29652. S. J. was supported by the Nuclear Science and Security Consortium (NSSC) that is funded by the DOE/NNSA under award number DE-NA0000979. E. M. was supported by the Nuclear Forensics Graduate Fellowship through the U.S. Department of Homeland Security and the U.S. Department of Defense. XAS measurements were carried out at the Stanford Synchrotron Radiation Lightsource, a directorate of SLAC National Accelerator Laboratory and an Office of Science User Facility operated for the U.S. DOE, Office of Science, by Stanford University. TEM measurements performed at LLNL were supported by the Subsurface Biogeochemical Research Program of the U.S. Department of Energy's Office of Biological and Environmental Research and performed under the auspices of the U.S. Department of Energy by Lawrence Livermore National Laboratory under Contract DE-AC52-07NA27344. The views and conclusions contained in this document are those of the authors and should not be interpreted as necessarily representing the official policies, either expressed or implied, of the U.S. Department of Homeland Security, the U.S. DOE, and the U.S. Department of Defense.

References

1. G. Choppin, *Journal of Radioanalytical and Nuclear Chemistry*, 2007, **273**, 695-703.
2. R. J. Silva and H. Nitsche, in *Advances in Plutonium Chemistry 1967-2000*, ed. D. C. Hoffman, American Nuclear Society, La Grange Park, IL, 2002, ch. 6, pp. 89-111.
3. R. J. Silva and H. Nitsche, *Radiochimica Acta*, 1995, **70-1**, 377-396.
4. W. Runde, *Los Alamos Science*, 2000, **26**, 392-411.
5. D. L. Clark, *Los Alamos Science*, 2000, **26**, 364-381.
6. A. B. Kersting, *Inorganic Chemistry*, 2013, **52**, 3533-3546.
7. H. A. Omar and H. Moloukhia, *Journal of Hazardous Materials*, 2008, **157**, 242-246.
8. H. M. H. Gad and N. S. Awwad, *Separation Science and Technology*, 2007, **42**, 3657-3680.
9. G. R. Choppin, *Journal of Alloys and Compounds*, 1995, **223**, 174-179.
10. A. Mellah, S. Chegrouche and M. Barkat, *Journal of Colloid and Interface Science*, 2006, **296**, 434-441.
11. L. N. Oji, W. R. Wilmarth and D. T. Hobbs, *Nuclear Technology*, 2010, **169**, 143-149.
12. M. T. V. Ganzerli, V. Crespi Caramella and L. Maggi, *Journal of Radioanalytical and Nuclear Chemistry*, 2002, **254**, 3-7.

13. M. T. V. Ganzerli, V. Crespi Caramella and L. Maggi, *Journal of Radioanalytical and Nuclear Chemistry*, 2004, **260**, 579-583.
14. H. H. Someda and R. R. Sheha, *Journal of Nuclear and Radiochemical Sciences*, 2006, **7**, 37-43.
15. H. H. Someda and R. R. Sheha, *Radiochemistry*, 2008, **50**, 56-63.
16. S. J. Coleman, P. R. Coronado, R. S. Maxwell and J. G. Reynolds, *Environmental Science & Technology*, 2003, **37**, 2286-2290.
17. A. M. Starvin and T. P. Rao, *Talanta*, 2004, **63**, 225-232.
18. Y. Zhao, C. Liu, M. Feng, Z. Chen, S. Li, G. Tian, L. Wang, J. Huang and S. Li, *Journal of Hazardous Materials*, **176**, 119-124.
19. M. Arisaka, M. Watanabe and T. Kimura, *Journal of Nuclear Materials*, 2010, **407**, 116-118.
20. X. Wang, C. Chen, W. Hu, A. Ding, D. Xu and X. Zhou, *Environmental Science & Technology*, 2005, **39**, 2856-2860.
21. O. B. Mokhodoeva, G. V. Myasoedova and E. A. Zakharchenko, *Radiochemistry*, 2011, **53**, 35-43.
22. S. A. Perevalov and N. P. Molochnikova, *Journal of Radioanalytical and Nuclear Chemistry*, 2009, **281**, 603-608.
23. G. V. Myasoedova, N. P. Molochnikova, A. G. Tkachev, E. N. Tugolukov, S. V. Mishchenko and B. F. Myasoedov, *Radiochemistry*, 2009, **51**, 156-158.
24. Q. H. Fan, D. D. Shao, J. Hu, C. L. Chen, W. S. Wu and X. K. Wang, *Radiochimica Acta*, 2009, **97**, 141-148.
25. C. L. Chen, J. Hu, D. Xu, X. L. Tan, Y. D. Meng and X. K. Wang, *Journal of Colloid and Interface Science*, 2008, **323**, 33-41.
26. Y. Sun, S. Yang, G. Sheng, Z. Guo and X. Wang, *Journal of Environmental Radioactivity*, 2012, **105**, 40-47.
27. Fasfous, II and J. N. Dawoud, *Applied Surface Science*, 2012, **259**, 433-440.
28. Y. B. Sun, Q. Wang, C. L. Chen, X. L. Tan and X. K. Wang, *Environmental Science & Technology*, 2012, **46**, 6020-6027.
29. A. Y. Romanchuk, A. S. Slesarev, S. N. Kalmykov, D. V. Kosynkin and J. M. Tour, *Physical Chemistry Chemical Physics*, 2013.
30. M. Carboni, C. W. Abney, K. M. L. Taylor-Pashow, J. L. Vivero-Escoto and W. Lin, *Industrial & Engineering Chemistry Research*, 2013, **52**, 15187-15197.
31. J. Gorka, R. T. Mayes, L. Baggetto, G. M. Veith and S. Dai, *Journal of Materials Chemistry A*, 2013, **1**, 3016-3026.
32. J. Kim, C. Tsouris, R. T. Mayes, Y. Oyola, T. Saito, C. J. Janke, S. Dai, E. Schneider and D. Sachde, *Separation Science and Technology*, 2013, **48**, 367-387.
33. Y. F. Yue, R. T. Mayes, J. Kim, P. F. Fulvio, X. G. Sun, C. Tsouris, J. H. Chen, S. Brown and S. Dai, *Angewandte Chemie-International Edition*, 2013, **52**, 13458-13462.
34. Y. Jung, S. Kim, S.-J. Park and J. M. Kim, *Colloids and Surfaces A: Physicochemical and Engineering Aspects*, 2008, **313–314**, 292-295.
35. Y. H. Liu, Q. Li, X. H. Cao, Y. Q. Wang, X. H. Jiang, M. Li, M. Hua and Z. B. Zhang, *Applied Surface Science*, 2013, **285**, 258-266.
36. Y. H. Liu, Y. Q. Wang, Z. B. Zhang, X. H. Cao, W. B. Nie, Q. Li and R. Hua, *Applied Surface Science*, 2013, **273**, 68-74.
37. X. D. Yang, J. Li, J. Liu, Y. Tian, B. Li, K. C. Cao, S. B. Liu, M. Hou, S. J. Li and L. J. Ma, *Journal of Materials Chemistry A*, 2014, **2**, 1550-1559.
38. Z. B. Zhang, X. H. Cao, P. Liang and Y. H. Liu, *Journal of Radioanalytical and Nuclear Chemistry*, 2013, **295**, 1201-1208.
39. Y. Q. Wang, Z. B. Zhang, Y. H. Liu, X. H. Cao, Y. T. Liu and Q. Li, *Chemical Engineering Journal*, 2012, **198**, 246-253.
40. B. W. Nie, Z. B. Zhang, X. H. Cao, Y. H. Liu and P. Liang, *Journal of Radioanalytical and Nuclear Chemistry*, 2013, **295**, 663-670.
41. G. Tian, J. Geng, Y. Jin, C. Wang, S. Li, Z. Chen, H. Wang, Y. Zhao and S. Li, *Journal of Hazardous Materials*, 2011, **190**, 442-450.
42. T. Parsons-Moss, H. Tüysüz, D. Wang, S. Jones, D. Olive and H. Nitsche, *Radiochimica Acta*, 2014, **102**, 489-504.
43. Y. Meng, D. Gu, F. Q. Zhang, Y. F. Shi, L. Cheng, D. Feng, Z. X. Wu, Z. X. Chen, Y. Wan, A. Stein and D. Y. Zhao, *Chemistry of Materials*, 2006, **18**, 4447-4464.
44. R. L. Liu, Y. F. Shi, Y. Wan, Y. Meng, F. Q. Zhang, D. Gu, Z. X. Chen, B. Tu and D. Y. Zhao, *Journal of the American Chemical Society*, 2006, **128**, 11652-11662.
45. Z. Wu, P. A. Webley and D. Zhao, *Langmuir*, 2010, **26**, 10277-10286.
46. E. Cristiano, Y.-J. Hu, M. Siegfried, D. Kaplan and H. Nitsche, *Clays and Clay Minerals*, 2011, **59**, 107-116.
47. J. M. Cleveland, *The Chemistry of Plutonium*, American Nuclear Society, La Grange Park, IL, 2nd edn., 1979.
48. T. W. Newton, D. E. Hobart and P. D. Palmer, *Radiochimica Acta*, 1986, **39**, 139-147.
49. Y.-J. Hu, L. Kestrel Schwaiger, C. H. Booth, R. K. Kukkadapu, E. Cristiano, D. Kaplan and H. Nitsche, *Radiochimica Acta*, 2010, **98**, 655-663.
50. P. J. Panak, C. H. Booth, D. L. Caulder, J. J. Bucher, D. K. Shuh and H. Nitsche, *Radiochimica Acta*, 2002, **90**, 315-321.
51. Z. R. Yue, W. Jiang, L. Wang, S. D. Gardner and C. U. Pittman Jr, *Carbon*, 1999, **37**, 1785-1796.
52. P. A. Bazula, A. H. Lu, J. J. Nitz and F. Schuth, *Microporous and Mesoporous Materials*, 2008, **108**, 266-275.
53. J. S. Noh and J. A. Schwarz, *Carbon*, 1990, **28**, 675-682.
54. M. R. McPhail, J. A. Sells, Z. He and C. C. Chusuei, *The Journal of Physical Chemistry C*, 2009, **113**, 14102-14109.
55. T. Moeller, *The Chemistry of the Lanthanides*, Reinhold, New York, 1963.
56. L. Y. Yuan, Y. L. Liu, W. Q. Shi, Y. L. Lv, J. H. Lan, Y. L. Zhao and Z. F. Chai, *Dalton Transactions*, 2011, **40**, 7446-7453.
57. G. A. Parks, in *Mineral-Water Interface Geochemistry*, ed. M. F. J. W. Hochella, Art F., Mineralogical Society of America, Washington, D.C., 1990, vol. 23, ch. 4, p. 603.
58. A. Y. Romanchuk, S. N. Kalmykov, A. V. Egorov, Y. V. Zubavichus, A. A. Shiryaev, O. N. Batuk, S. D. Conradson, D. A. Pankratov and I. A. Presnyakov, *Geochimica et Cosmochimica Acta*, 2013, **121**, 29-40.
59. B. A. Powell, Z. R. Dai, M. Zavarin, P. H. Zhao and A. B. Kersting, *Environmental Science & Technology*, 2011, **45**, 2698-2703.
60. W. Teng, Z. X. Wu, J. W. Fan, H. Chen, D. Feng, Y. Y. Lv, J. X. Wang, A. M. Asiri and D. Y. Zhao, *Energy & Environmental Science*, 2013, **6**, 2765-2776.